Backbone Dynamics, Amide Hydrogen Exchange, and Resonance Assignments of the DNA Methylphosphotriester Repair Domain of Escherichia coli Ada Using NMR †

5 AUTHORS, INCLUDING:

Judith Habazettl
University of Basel
15 PUBLICATIONS **522** CITATIONS

SEE PROFILE

Gregory L Verdine
Harvard University
229 PUBLICATIONS **16,879** CITATIONS

SEE PROFILE

Gerhard Wagner
Harvard Medical School
519 PUBLICATIONS **35,500** CITATIONS

SEE PROFILE

Backbone Dynamics, Amide Hydrogen Exchange, and Resonance Assignments of the DNA Methylphosphotriester Repair Domain of *Escherichia coli* Ada Using NMR[†]

Judith Habazettl,[‡] Lawrence C. Myers,[§] Feng Yuan,[‡] Gregory L. Verdine,[§,||] and Gerhard Wagner*,[‡,§]

Department of Biological Chemistry and Molecular Pharmacology, Harvard Medical School, Boston, Massachusetts 02115, and Program for Higher Degrees in Biophysics and Department of Chemistry, Harvard University, Cambridge, Massachusetts 02138

ABSTRACT: The 10 kDa amino-terminal fragment of *Escherichia coli* Ada protein (N-Ada10) repairs methyl phosphotriesters in DNA and possesses a tightly bound zinc ion. The complete resonance assignments of this protein domain have been obtained using multidimensional homonuclear and heteronuclear NMR experiments. The assignments served to study the internal mobility of this protein domain via ^{15}N relaxation experiments. This involved the measurement of longitudinal and transverse ^{15}N relaxation rates, as well as the amide proton solvent exchange rates. Relaxation rates in the rotating frame, $R_{1\rho}$, of ^{15}N nuclei were measured at different spin-lock field strengths, leading to the detection of two slow conformational exchange processes at Gly-25 and Gln-73. For the latter, which is next to the active site of this protein domain, the characteristic time of this process was found to be around 60 μs. The other relaxation experiments unveiled some regions of fast internal motions, faster than the overall correlation time. These motions were found in the N- and C- terminal tails, in segment 33−35 which forms the turn between β-strands S1 and S2, and residues 47−52 located in a long loop preceding strand S3. The latter loop belongs to the potential DNA binding surface of N-Ada10. While the structure from residue 18 to residue 26 appears not well defined in the calculated structure, the relaxation experiments do not indicate higher mobility for this region. Residues at the N-terminal portion, including the first helix, the sequentially adjacent loop, and part of the second helix, exhibit internal motions close to the time scale of the overall rotational correlation time. This appears to be related to the fact that the first helix has no hydrogen bonds or salt bridges to the rest of the protein and is stabilized only by the involvement of some of its side chains in a hydrophobic core consisting of the side chains of two phenylalanines, a tryptophan, a leucine, and a valine. The four cysteines which bind the zinc show motions on different time scales ranging from microseconds to picoseconds. Thus the motions in the immediate region around the bound zinc of the DNA methyl phosphotriester repair domain are of relatively small amplitude but take place over a wide time range. On the other hand, high mobility is found in the turn connecting S1 and S2 and in the loop preceding S3, regions of the potential DNA binding surface.

Escherichia coli Ada repairs the mutagenic lesion O^6-methylguanine by direct, irreversible transfer of the methyl group to a cysteine residue in the C-terminal protein domain. Ada also repairs the S_p diastereomer of DNA methyl phosphotriesters by direct methyl transfer to another cysteine residue, Cys-69, located in the N-terminal domain (Demple, 1990). Methylation of Cys-69 reveals a strong sequence-specific DNA binding activity in the N-terminal domain, which enables Ada to activate transcription of a methylation-resistance regulon. The methylated Ada protein activates transcription of the *ada* gene as well as several other genes that encode DNA repair functions. Hence, aside from its

direct role in the repair of mutagenic DNA lesions, Ada acts as a chemosensor for methylation damage in the cell (Lindahl et al., 1988).

The N-terminal domain of Ada possesses a tightly bound zinc ion that is necessary for proper folding *in vitro* and *in vivo* (Myers et al., 1992). ^{113}Cd nuclear magnetic resonance (NMR)[1] studies on Ada fragments revealed an unusual Cys-X_3-Cys-X_{26}-Cys-X_2-Cys ligand arrangement (Myers et al., 1993a,b). One of the four ligand residues in Ada was identified as Cys-69, thereby implicating the zinc ion not only in stabilization of the protein structure but also in direct metalloactivation of the methyl acceptor residue (Myers et al., 1993b). The methylation of Cys-69 substantially enhances the sequence-specific DNA binding by Ada, decreasing the K_d by a factor of ≈1000 (Myers et al., 1995). It appears, however, that the structural switch resulting in this

---

[‡] Department of Biological Chemistry and Molecular Pharmacology.
[§] Program for Higher Degrees in Biophysics.
[||] Department of Chemistry.
[⊗] Abstract published in *Advance ACS Abstracts,* July 1, 1996.

[1] Abbreviations: N-Ada10, Ada fragment containing residues 1−92; NMR, nuclear magnetic resonance; M9-glc, M9 minimal media supplemented with glucose; TOCSY, total correlation spectroscopy; NOESY, nuclear Overhauser effect spectroscopy, HMQC, heteronuclear multiple-quantum coherence spectroscopy; DQF-COSY, double-quantum-filtered correlation spectroscopy; HSQC, 2D ^{15}N–^{1}H heteronuclear single-quantum coherence spectroscopy; 2D, two dimensional.
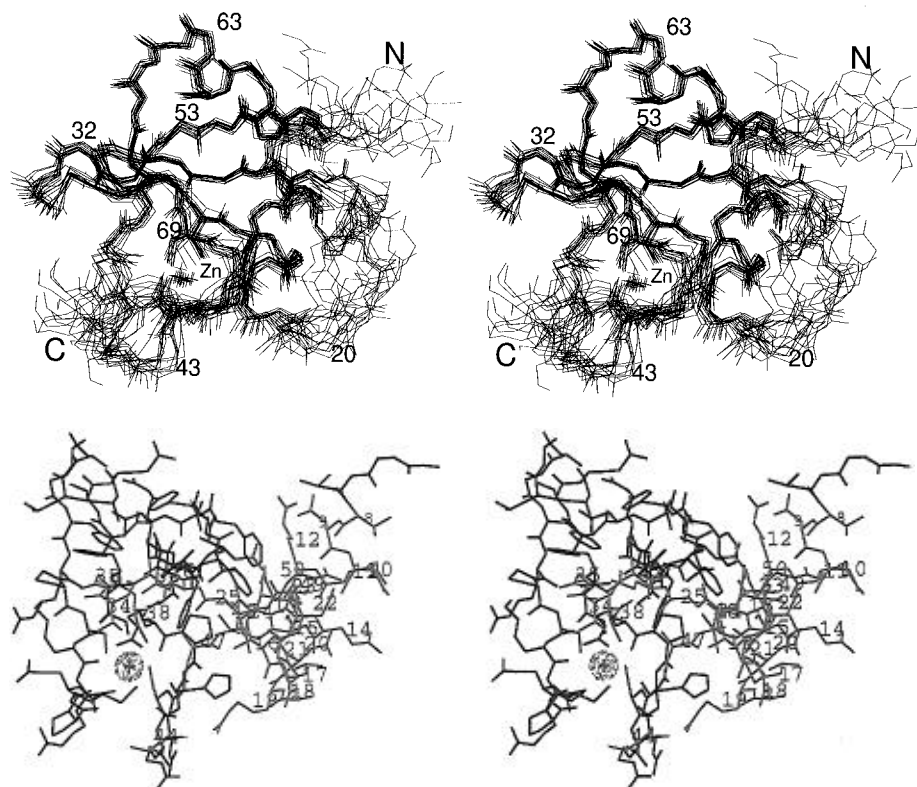
FIGURE 1: Solution structure of N-Ada10 (Myers et al., 1993b, PDB code 1ADN). (A, top) Stereoview of the overlay of 14 final structures of N-Ada10 (residues 5−75). All backbone heavy atoms, the zinc binding cysteine side chains, and the zinc atom marked by a cross are shown. The zinc binding cysteines are, clockwise, Cys-69, Cys-72, Cys-42, and Cys-38. The proximal NH_2 and COOH termini are labeled N and C, respectively. (B, bottom) Single representative model from the ensemble with all heavy atoms shown (residues 5−75). The location of the zinc and the cysteine side chains involved in metal binding are shown in red. Residues with motional components in the time range of τ_m are shown in magenta (residues 8−26, 33−35, 38, 44, and 47−50). They constitute a nearly contiguous wedge penetrating the protein from the right.

increase in binding affinity does not involve the dissociation of the methylated cysteine from the metal (Ohkubo et al., 1994; Myers et al., 1994).

The zinc binding and DNA methyl phosphotriester repair functionality is completely retained in a 10 kDa fragment of the N-terminus of Ada (Myers et al., 1992) comprising residues 1−92 (N-Ada10). N-Ada10 lacks, however, residues essential for sequence-specific DNA binding (Sakashita et al., 1993; Myers et al., 1994a). The solution structure of N-Ada10 has been determined by NMR (Myers et al., 1993b; PDB access code 1ADN) and has a global fold consisting of three well-defined layers of secondary structure consisting of a β-sheet sandwiched between two α-helices (Figure 1). The zinc binding pocket of N-Ada10 lies on the edge of the β-sheet and is formed by two parallel strands of β-sheet and two parallel loops which extend from each strand, turning under the β-sheet. Two of the zinc ligands, Cys-69 and Cys-38, are positioned across from one another of the β-sheet while the remaining ligands, Cys-42 and Cys-72, are located on the loops. However, the structure around residues Cys-42 and Cys-72 could not be well defined with NMR due to lack of NOEs.

The measurement of ^{15}N and ^{13}C NMR relaxation rates provides information about the internal dynamics of proteins on time scales faster than the rotational correlation time [see for a review Wagner (1993)]. Within the last several years, NMR relaxation studies have been carried out for ^{13}C nuclei at natural abundance in BPTI (Nirmala & Wagner, 1988), cyclosporin A (Dellwo & Wand, 1989), and an Xfin zinc finger (Palmer et al., 1991). Relaxation studies have also been carried out for amide ^{15}N nuclei in uniformly enriched

staphylococcal nuclei (Kay et al., 1989), interleukin-1β (Clore et al., 1990b), the IIA domain of a glucose permease (Stone et al., 1992), calcium-loaded calbindin D_{9k} (Kördel et al., 1992), eglin c (Peng et al., 1992b), interleukin-4 (Redfield et al., 1992), ubiquitin (Schneider et al., 1992), ribonuclease H (Powers et al., 1992), calmodulin (Barbato et al., 1992), reduced and oxidized thioredoxin (Stone et al., 1993), interleukin-8 (Grasberger et al., 1993), urokinase (Nowak et al., 1993), BPTI (Szyperski et al., 1993), ribonuclease T1 and its complex (Fushman et al., 1994), apo- and holo-acyl-coenzyme A binding protein (Rischel et al., 1994), and granulocyte colony-stimulating factor (Zink et al., 1994). Generally, the ^{15}N relaxation data are interpreted with either the model-free approach (Lipari & Szabo, 1982), the extended model-free approach (Clore et al., 1990a), or specific motional models, such as the wobbling-in-a-cone model (Woessner, 1962; Kinoshita et al., 1977). These approaches make assumptions about the analytical form of the power spectral density function $J(\omega)$. These analytical forms depend on a few parameters, such as correlation times and order parameters in the "model-free approach", or cone angles and diffusion constants in the "wobbling-in-the-cone" model. The relaxation rates can then be expressed directly in terms of these parameters, without further consideration of the shape of the spectral density function. Alternatively, it has been proposed to map the spectral density function directly from a combination of relaxation parameters prior to a fit to an analytical expression of $J(\omega)$ (Peng et al., 1992a,b), and the resulting values of the spectral density function can be fitted afterward to more specific models. In all cases at least three experimental parameters are needed,

R_1, R_2, and heteronuclear NOEs. The heteronuclear NOEs, however, are difficult to measure accurately, due to the reduced sensitivity of the NOE experiment. Therefore, the NOE is often used only in a qualitative way, and the order parameter S^2 and the overall correlation time τ_c are estimated using only R_1 and R_2 (Kay et al., 1989; Habazettl & Wagner, 1995).

Slow conformational exchange in the time range of microseconds can be studied with measurements of relaxation rates in the rotating frame, $R_{1\rho}$, of spin-locked magnetization as a function of the strength of the spin-locking field (Deverell et al., 1969) or with the Carr–Purcell–Meiboom–Gill spin-echo decay rate as a function of the repetition rate of the refocusing pulses (Meiboom & Gill, 1958; Carr & Purcell, 1954). The latest applications of these methods included the characterization of a conformational exchange rate that was claimed to be related to the isomerization of the chirality of a disulfide bond in BPTI (Szyperski et al., 1993), as well as the determination of the dissociation rate constant for an inhibitor–enzyme complex (Davis et al., 1994). Complementary information about the stability and dynamics of proteins can be gained by measuring amide hydrogen exchange rates with NMR spectroscopy (Wagner, 1983; Englander &Kallenbach, 1984).

In this study we report on the assignment of the proton, nitrogen, and carbon resonances of N-Ada10 at 25 °C. In addition, we investigate the dynamics and stability of the protein. Two-dimensional inverse-detected heteronuclear $^{15}N–H$ NMR spectroscopy has been used to measure the longitudinal and the transverse relaxation rates, R_1 and R_2, respectively, for the backbone nitrogens at 25 °C and 500 MHz. Slow conformational exchange processes have been identified at two sites of the protein, at Gly-25 and Gln-73. The time constant of that exchange process at Gln-73 has been determined by $R_{1\rho}$ relaxation rate measurements at different spin-lock field strengths. The backbone amide proton exchange rates of N-Ada10 with solvent have been derived using $^1H–^{15}N$ heteronuclear correlation NMR spectroscopy and compared with the results from the relaxation experiments. The results have been analyzed together with the amide proton exchange rates in a semiquantitative way based on procedures developed previously (Habazettl & Wagner, 1995).

METHODS

Production and Purification of N-Ada10. Unlabeled N-Ada10 protein and the uniformly ^{15}N-labeled N-Ada10 fragment were expressed and purified as previously described (Myers et al., 1992, 1993a). The uniformly $^{15}N,^{13}C$-labeled N-Ada10 was obtained by growing the cells in M9-glc minimal medium containing $^{15}NH_4Cl$ and $[^{13}C]$glucose (Cambridge Isotopes) as the sole nitrogen and carbon sources, respectively. To obtain the zinc form of N-Ada10, the M9-glc minimal medium was supplemented with $ZnCl_2$ (100 μM). The purified protein samples were exchanged into a buffer containing 25 mM sodium phosphate, 50 mM NaCl, and 10 mM 2-mercaptoethanol, pH 6.4, and concentrated to 2–3 mM in protein. The concentrated samples were lyophilized, resuspended in an equal volume of degassed 95% H_2O/5% D_2O or D_2O (99.99%) under argon in a 5 mm NMR tube for NMR measurements.

NMR Spectroscopy for Assigning N-Ada10. Measurements were made on a Bruker AMX-500 or AMX-600

spectrometer using 2–3 mM N-Ada10 samples at pH 6.4 and 25 °C. The pH of the D_2O samples was adjusted for the isotope effects. In all experiments the ^1H carrier was placed on the water line, and presaturation during the recycle delay was used for all samples requiring water suppression. Unless otherwise stated, time-proportional phase incrementation (TPPI) was used for sign discrimination along the indirect dimensions. Data were processed using Felix software (Biosym Technologies, San Diego, CA).

Sequential connectivities of backbone resonances were established using HNCA (Kay et al., 1990) and HN(CO)-CA (Bax & Ikura, 1991) adapted for constant time in the ^{15}N dimension (Grzesiek & Bax, 1992) on the uniformly labeled $^{15}N,^{13}C$ N-Ada10 sample in H_2O. The HNCA experiment was executed with spectral widths of 32.9, 24, and 13.89 ppm in $F_1(^{15}N)$, $F_2(^{13}C)$, and $F_3(^1H)$, respectively, and with 45 real points in t_1, 128 real points in t_2, and 512 complex points in t_3 at 16 scans per point. The ^{15}N and ^{13}C carriers were positioned at 118.3 and 50.0 ppm, respectively. The HN(CO)CA experiment was conducted with parameters identical to those of the HNCA above with the exception that 50 real points were collected in t_1 (^{15}N).

The identification of spin system types and side-chain resonance assignments was determined using a combination of total correlation spectroscopy (TOCSY) and nuclear Overhauser effect spectroscopy (NOESY). A 3D ^{15}N TOCSY-HMQC experiment (Marion et al., 1989) was acquired using the uniformly ^{15}N-labeled N-Ada10 sample in H_2O, with a SCUBA recovery (Brown et al., 1988) after the presaturation of the water. This experiment had spectral widths of 13.89 ppm in both $F_1(^1H)$ and $F_3(^1H)$ and 32.9 ppm in $F_2(^{15}N)$ and was collected with 256 real points in t_1, 32 real points in t_2, and 512 complex points in t_3 at 32 scans per point. The ^{15}N carrier was located at 118.3 ppm. A 3D HCCH TOCSY utilizing heteronuclear cross-polarization (Zuiderweg, 1990) was acquired on the uniformly labeled $^{15}N,^{13}C$ N-Ada10 sample using a DIPSI-3 spin lock. This experiment had spectral widths of 16 ppm in $F_1(^1H)$, 24.99 ppm in $F_3(^1H)$, and 65 ppm in $F_2(^{13}C)$ and was collected with 256 complex points in t_1, 64 real points in t_2, and 512 complex points in t_3 at eight scans per point. The ^{13}C carrier was placed at 40 ppm. A 3D ^{15}N NOESY-HMQC experiment (Fesik & Zuiderweg, 1988) was carried out with identical sample and spectroscopic conditions and included a SCUBA recovery during the 100 ms mixing time. In addition, a 3D ^{13}C NOESY-HMQC experiment was conducted with the uniformly labeled $^{15}N,^{13}C$ N-Ada10 sample in D_2O. This experiment had spectral widths of 12.00 ppm in $F_1(^1H)$, 24.99 ppm in $F_3(^1H)$, and 65 ppm in $F_2(^{13}C)$ and was collected using TPPI–States cycling for data collection with 256 complex points in t_1, 52 real points in t_2, and 512 complex points in t_3 at eight scans per point. The experiment used a 100 ms NOESY mixing time, and the ^{13}C carrier was located at 40.0 ppm.

Two-dimensional $^{15}N–^1H$ and $^{13}C–^1H$ heteronuclear single-quantum coherence (HSQC) spectroscopy (Bodenhausen & Ruben, 1980) NMR spectra were acquired to assist in the interpretation of the heteronuclear 3D data. The 2D $^{15}N–^1H$ HSQC spectrum was recorded using the uniformly ^{15}N-labeled N-Ada10 sample in H_2O, with a SCUBA recovery after the presaturation of the water. The ^{15}N carrier was positioned at 118.3 ppm, and sweep widths were 32.9 ppm in $F_1(^{15}N)$ and 13.89 ppm in $F_2(^1H)$. The 2D $^{13}C–^1H$ HSQC spectrum was recorded using the uniformly $^{15}N,^{13}C$-

labeled N-Ada10 sample in D_2O and the ^{13}C carrier positioned at 40 ppm. The sweep widths were 100 ppm in $F_1(^{13}C)$ and 13.89 ppm in $F_2(^{1}H)$ with 497 real points in t_1 and 2048 complex points in t_2 collected at 48 scans per point. A second 2D $^{13}C-^{1}H$ HSQC spectrum was recorded on a 10% ^{13}C-labeled sample using identical parameters.

Several homonuclear experiments also aided the assignment of side-chain resonances. A 2D homonuclear TOCSY experiment was run on unlabeled samples of N-Ada10 in both H_2O and D_2O using presaturation of the water with a SCUBA recovery when appropriate. Both spectra utilized sweep widths of 13.89 ppm in $F_1(^{1}H)$ and $F_2(^{1}H)$ with 512 real points in t_1 and 2048 complex points in t_2 collected at 96 scans per point. Both spectra also used a DIPSI-2 spin-lock sequence in which TOCSY mixing times of 35, 52, 75, and 98 ms coadded. A 2D homonuclear NOESY experiment was run on unlabeled samples of N-Ada10 in both H_2O and D_2O using presaturation of the water with a SCUBA recovery when appropriate. The H_2O spectrum utilized sweep widths of 13.89 ppm in $F_1(^{1}H)$ and $F_2(^{1}H)$ with 512 real points in t_1 and 2048 complex points in t_2 collected at 96 scans per point. Both NOESY spectra were collected under identical conditions and 100 ms mixing times with the exception that 256 scans per point were used for the D_2O spectrum. A double-quantum-filtered correlation spectroscopy (DQF-COSY) (Piantini et al., 1982; Müller et al., 1986) spectrum of N-Ada10 in D_2O was used to assign both side-chain resonances and coupling constants. The DQF-COSY spectrum utilized sweep widths of 10.66 ppm in $F_1(^{1}H)$ and 13.89 ppm in $F_2(^{1}H)$ with 800 real points in t_1 and 2048 complex points in t_2 collected at 128 scans per point.

Stereospecific assignments of seven β-methylene groups were based on $C^{\alpha}H$ to $C^{\beta}H$ coupling constants obtained in DQF-COSY, intraresidue NOE data, and ^{15}N to $C^{\beta}H$ coupling constants estimated from a ^{1}H (TOCSY) on the ^{15}N-labeled sample (Montelione et al., 1989). Stereospecific assignments of all, but one pair of, valine and leucine methyl groups were obtained from the 2D $^{13}C-^{1}H$ HSQC spectrum recorded on the 10% ^{13}C-labeled sample (Neri et al., 1989; Senn et al., 1989; Szyperski et al., 1992).

NMR Spectroscopy for Measuring ^{15}N Relaxation Rates and NH Exchange Rates. All NMR experiments were carried out at 25 °C, on a Bruker AMX-500 spectrometer. The two relaxation parameters of the backbone NH bond vectors of N-Ada10 were measured as described elsewhere (Peng & Wagner, 1992a). The measured relaxation parameters included the longitudinal ^{15}N relaxation rate R_1 and the transverse ^{15}N relaxation rate $R_{1\rho}^{\text{eff}}$). The experiments use refocused INEPT heteronuclear correlation sequences for transferring the magnetization from the NH protons to the nitrogens or vice versa. While acquiring the proton magnetization, the nitrogen magnetization is broad-band decoupled with the GARP scheme (Shaka et al., 1995). In every pulse sequence a certain kind of nonequilibrium spin order is created, and its relaxation is monitored by recording a sequence of 2D spectra as a function of this relaxation delay. The relaxation rate for every amide N–NH vector is then determined from the decay of the intensity of the corresponding ^{15}N–NH cross peak in this sequence. All experiments were recorded with a spectral sweep width of 7042 Hz in the F_2 dimension with the carrier on the water signal. In the F_1 dimension the spectral width was set to 1622 Hz with the carrier in the center of the amide nitrogen

region. A total of 512 blocks in t_1, each of 2048 real data points, were recorded. Every free induction decay was comprised of eight scans. The measuring time for every 2D spectrum was approximately 3 h. Sign discrimination in F_1 was obtained by using the TPPI method of Marion and Wüthrich (1983). The R_1 rate was obtained by using 11 delays of 12, 2006, 403, 102, 601, 3508, 202, 1004, 803, 302, and 12 ms in the preceding order. The $R_{1\rho}^{\text{eff}}$ measurements also used 11 delays of 6.42, 180, 12.8, 154.2, 25.7, 128.5, 51.4, 77.1, 102.8, 12.8, and 38.5 ms. The ^{15}N spin-lock power in the relaxation delay was set to 2500 Hz, resulting in an effective field that was tipped between 90° and 74.25° from the laboratory z axis, for resonances between the center and the extreme edges of the spectrum, respectively.

The conformational exchange rate of residue Gln-73 was determined using the pulse sequences shown in Figure 2. These experiments measure the in-phase transverse relaxation rates, $R_{1\rho}$, as a function of the spin-lock field strength. As the B_1 field strength variations are negligible compared to the steady magnetic field B_0, contributions from the chemical shift anisotropy (CSA) do not affect the determination of the conformational exchange rate. For this reason, and to avoid complications at low spin-lock power, we did not attempt to eliminate effects of cross-correlation between CSA and dipolar interactions, as described in other studies of transverse relaxation rates (Palmer et al., 1992; Kay et al., 1992, Peng & Wagner, 1992a). A low-power continuous on-resonance spin lock was used to maintain transverse N_x magnetization for the relaxation delay T. To avoid off-resonance effects, the spin lock was placed on-resonance for this experiment. The transverse relaxation rates were determined with the pulse sequence of Figure 2A at spin lock powers of 3770, 6283, 9425, 11310, 13195, 15708, and 17593 rad s^{-1}. At spin-lock powers of 6283, 9425, and 15708 rad s^{-1}, relaxation delays of 6.4, 154.2, 77.1, 25.7, 102.8, 51.4, 128.5, and 6.4 ms were used in the preceding order. At the remaining spin-lock fields the preceding relaxation delays except the one at 128.5 ms were used. At spin-lock powers of 2513 and 6283 rad s^{-1} the pulse sequence of Figure 2B was applied. Since the CW spin lock decouples the ^{15}N nuclei and amide protons during the relaxation delay at higher powers, no additional decoupling of the NH protons is necessary. However, decoupling of the protons with Waltz-16 (Shaka et al., 1983) at lower spin-lock power improved the experimental performance. At the spin lock power of 6283 rad s^{-1} seven experiments ($T = 7.9, 103, 47.5, 150.5, 79.2, 23.76, 126.7$ ms) and at the spin-lock power of 2513 rad s^{-1} six experiments ($T = 7.9, 103, 47.5, 150.5, 79.2, 13.8, 126.7$ ms) were performed.

For the amide proton exchange experiments the protein sample in H_2O buffer was lyophilized. The exchange-out was initiated by dissolving the sample in degassed D_2O under argon to prevent oxidation of the cysteines. Data acquisition was started after a delay of 12 min to allow for sample preparation, temperature equilibration, stabilization of the lock signal, and quick shimming. A series of ^{1}H-detected $^{15}N-^{1}H$ correlation spectra were then collected for 2 days. The pulse sequence used incorporates a double INEPT transfer of magnetization from ^{1}H to ^{15}N and back again, known as the "Overbodenhausen" experiment (Bodenhausen & Ruben, 1980). The water resonance was suppressed with a trim pulse applied prior of magnetization transfer to ^{15}N
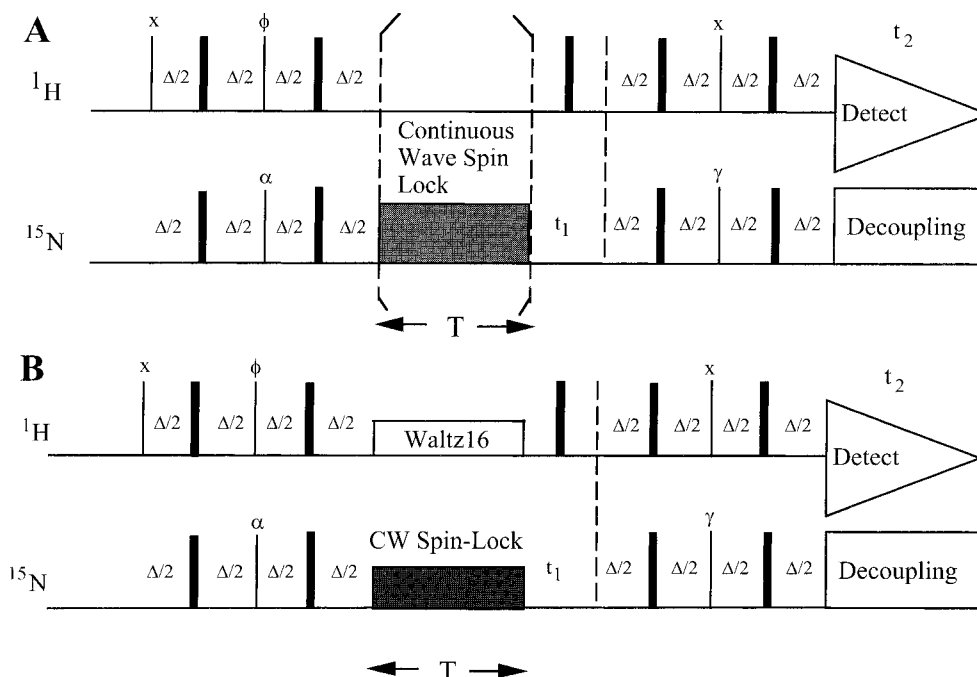
FIGURE 2: Two-dimensional heteronuclear pulse sequences for measuring the transverse relaxation rate $R_{1\rho}^{\text{eff}}$. The upper trace indicates proton pulses while the lower trace indicates the ^{15}N spin pulses. Pulses of 90° and 180° are shown as thin and thick vertical bars, respectively. $\Delta/2$ was set to $1/(4J_{\text{NH}}) = 2.75$ ms. The TPPI phase modulation is done on the first 90° ^{15}N pulse following the t_1 period. Pulse phases are shown above the pulses themselves with $\alpha = +x, -x$; $\phi = 4(+y), 4(-y)$; $\gamma = +x, +x, -x, -x$. In sequence B Waltz-16 composite pulse decoupling was applied on the protons during the continuous wave spin lock of the ^{15}N magnetization. The continuous wave spin-lock strength was varied.

(Messerle et al., 1989). The spectra were recorded with a sweep width of 7042 Hz in the F_2 dimension. A total of 128 increments, each of 1024 data points and two transients, were recorded, giving a sweep width of 2294 Hz in the F_1 dimension and a total experiment time of 4 min and 16 s. A total of 120 spectra were recorded on the first two days: blocks of 20 spectra were acquired with changing delays of 5 ms, 300 s, 600 s, 900 s, 1500 s, and 3600 s between the single experiments.

Data Processing Involving Relaxation Rates and NH Exchange Experiments. All data were processed on a SUN SLC workstation using FELIX 2.0 software provided by Dennis Hare (Hare Research, Seattle). Prior to Fourier transformation the data were multiplied with a 90° or with a 30° shifted sine-bell function in both dimensions. The resolution enhanced spectra were used to analyze cross peaks in crowded regions. The relaxation rates obtained were the same for both apodization functions [see also Skelton et al. (1993)]. An example of a representative 2D spectrum is shown in Figure 3.

Determination of Relaxation Rates and NH Exchange Rates. The intensity of cross peaks was obtained by selecting a slice in the F_2 dimension, through the maximum of the peak, applying a linear baseline correction, and integrating along this dimension. For every ^{15}N$-^1$H cross peak the intensities in dependence of the relaxation delay T or time point of the NH exchange experiments are fit to exponential decays using the Levenburg–Marquardt algorithm (Marquardt, 1963; Press et al., 1988):

$$I(T) = A + B \exp[-RT] \qquad (1)$$

For the longitudinal ^{15}N relaxation $R = R_1$, $A + B$ is the initial peak intensity and B the steady-state value. For the transverse relaxation rate and the NH exchange rate A is equal to zero and B is the initial value of the intensity.
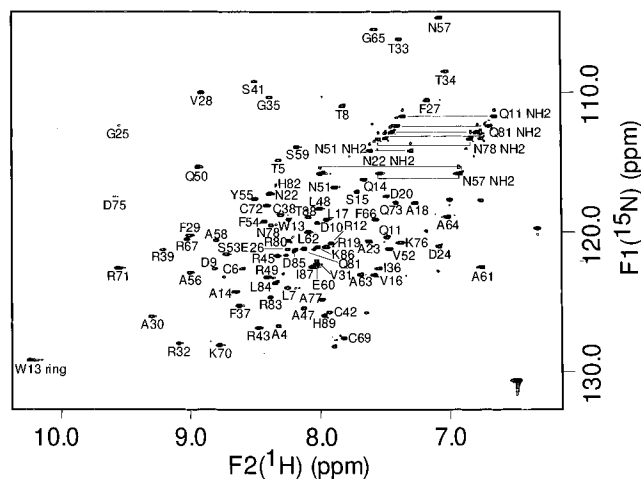

FIGURE 3: ^{15}N$-^1$H HSQC spectrum of N-Ada10. Assigned cross peaks for backbone amide protons and nitrogens are labeled by amino acid type and sequence number. The amide side-chain protons of asparagine and glutamine are connected by horizontal lines and labeled. The single tryptophan pyrrole proton has also been labeled. Several of the unlabeled peaks in the spectrum belong to the side-chain proton of arginine, which were folded into the spectrum.

In order to estimate the uncertainties in the relaxation rates or NH exchange rates, Monte Carlo simulations were performed (Palmer et al., 1991; Peng & Wagner, 1992b): assuming that the intensities are the means of Gaussian distributions and using the root mean square deviations between the experimental data and the optimized fits for the standard deviations of the Gaussians, 1000 synthetic data sets were generated for each cross peak. Of these simulated data the relaxation rates were determined with the Levenburg–Marquardt algorithm, and the standard deviation of this fit was taken as the estimated error of the relaxation rate. Errors originating from uncertainties in the one-dimensional cross-peak integrals are typically of the same

magnitude or less than those derived from the fitting routine (Peng & Wagner, 1992b). Using a repeated data value for estimating the random errors in the determination of the relaxation rates (Palmer et al., 1992) resulted also in smaller errors. Since the protein is not very stable in solution, the intensity of the first data point that was repeated after the experiment was typically reduced by 2% after 30 h. As the spectra were acquired in random order, errors stemming from protein instability were included in the fit of the data.

For the analysis of relaxation of in-phase coherence in the rotating frame we made the following approximations: For an on-resonance but weak spin lock ($\gamma B_1 = \omega_{SL}$), $R_{1\rho}$ is approximately identical to R_2 (Peng et al., 1991). For this to be true it is also assumed that the spectral density functions are Lorentzians. If the frequency of exchange between different sites is $\omega_e \ll 1/\tau_m$, and the spin lock is nearly but not exactly on-resonance, the relaxation rates in the rotating frame, $R_{1\rho}^{eff}$, are approximately a linear combination of longitudinal and transverse relaxation due to resonance offset effects (Peng et al., 1991; Peng & Wagner, 1994a,b; Davis et al., 1994):

$$R_{1\rho}^{eff} = R_1 \cos^2(\beta) + R_{1\rho} \sin^2(\beta) \qquad (2)$$

where $\cos(\beta) = \Delta\omega/\omega_e$, $\omega_e = (\Delta\omega_0^2 + \omega_{SL}^2)^{1/2}$, $\Delta\omega$ is the offset between the carrier and the resonance frequency, and $\omega_0 = \gamma B_0$. The ^{15}N spin-lock power $\omega_{SL} = 15\,708$ rad s^{-1} resulted in an effective field with $\beta = 74.25°$ from the laboratory z axis for resonances at the extreme edges of the spectrum. For residue Asn-57 the neglect of offset effects would result in an error of 6%, with $R_{1\rho}^{eff} = 10.12 \pm 0.14$ s^{-1} and $R_{1\rho} = 10.78 \pm 0.15$ s^{-1}. Therefore, the $R_{1\rho}$ values for all residues were calculated with eq 2, using the experimental values of $R_{1\rho}^{eff}$ and R_1. From now on we will designate $R_{1\rho}$ with R_2.

RESULTS

Resonance Assignments. Sequential resonance assignments were obtained from HNCA and HN(CO)CA experiments recorded on uniformly labeled ^{15}N- and ^{13}C-labeled N-Ada10 and from homonuclear TOCSY and NOESY spectra recorded on unlabeled protein. As is apparent in the 2D ^{15}N$-^1$H HSQC spectrum (Figure 3), N-Ada10 shows a good spectral dispersion of both amide backbone protons and nitrogen with only two or three cases of substantial overlap. In addition, the 2D ^{13}C$-^1$H HSQC spectrum of N-Ada10 was also remarkably well resolved. Thus, HNCA and HN(CO)CA resolved any issues of overlap and provided sequential connectivities for almost all of the assigned backbone resonances of N-Ada10, with the exception of residues preceding prolines and those which were undergoing fast exchange with the solvent. In this manner, a total of 75 explicit sequential connectivities were made using HN-(CO)CA, 64 of which were also identified as the secondary correlation to the preceding residue in the HNCA experiment. Backbone assignments could not be made for the first and last three residues.

Short-range NOE data assisted in making the sequential assignments in positions which the HN(CO)CA did not provide and helped to confirm those supplied by HN(CO)-CA. The assignment of the long-chain hydrophobic residues was also achieved to near completion using the ^{13}C-dispersed NOESY and TOCSY data. The leucine and valine methyl groups were easily assigned in the 2D ^{13}C$-^1$H HSQC
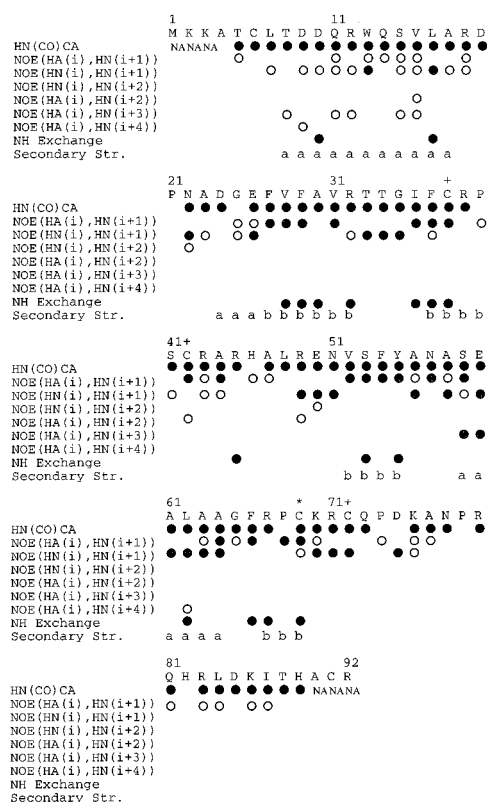
FIGURE 4: Summary of sequential connectivities and secondary structure for N-Ada10. The numbers in the top two rows correspond to the sequence number and residue type of each amino acid component of N-Ada10, respectively. A (+) above a residue indicates that it is a zinc ligand, while an (*) indicates the active site and zinc ligand Cys-69. The third row designated HN(CO)CA summarizes all the (i) to ($i-1$) connectivities found in the HN-(CO)CA experiment and marks the presence of each with a filled-in black circle. The presence of an "NA" in this row means that no resonances for the particular residue have been assigned. The following six rows display sequential and medium-range backbone NOE information relevant to connectivities determined in the HNCA and HN(CO)CA experiments and secondary structure. A filled circle in any of these rows represents the presence of a strong NOE, and a open circle represents the presence of a medium-strength NOE cross peak. The second to last row indicates amide backbone protons which are slowly exchanging, indicated with a filled circle. The final row represents the presence of defined secondary structure elements where an "a" indicates an α-helix and a "b" indicates a β-sheet.

spectrum which in turn permitted the stereospecific assignments for eight of the nine pairs of methyl groups using the 2D ^{13}C$-^1$H HSQC spectrum of the 10% ^{13}C-labeled samples. Many outer protons on arginine and lysine residues, both of which make up a substantial fraction of N-Ada10, could not be assigned. Problems with the assignment of these protons were in part a result of spectral overlap; however, in many cases with the extra dispersion of the 3D ^{13}C TOCSY spectrum the correlations among the outer protons of these side chains could simply not be observed. A summary of the data used for the sequential assignments is given in Figure 4; a list of the assignments is available in the Supporting Information.

Analysis of Relaxation Rates of N-Ada10. The relaxation rates of the amide ^{15}N spins in proteins are primarily dominated by (i) the dipolar coupling of the ^{15}N nucleus with the amide proton modulated by the rotational fluctuations of this N$-$NH vector in the external magnetic field and (ii) the chemical shift anisotropy and the rotational fluctuations of this ^{15}N chemical shift tensor in the external magnetic

field. (iii) Chemical exchange may also contribute to transverse relaxation rates, usually only for a small subset of resonances. These rotational fluctuations can be described with an angular autocorrelation function $G(t)$, which describes the correlation between the orientation of the N−H vector at time t and $t + \tau$ in an ensemble of molecules. The Fourier cosine transform of $G(t)$ then yields the *relative* frequency portion of $G(t)$, the rotational spectral density function $J(\omega)$. Therefore, the more internal high-frequency motion a N−NH vector experiences, the smaller is $J(0)$ and vice versa. The relaxation rates of the amide ^{15}N spin are linear combinations of this spectral density function at different frequencies (Abragam, 1961)

$$R_1 = d\{J(\omega_H - \omega_N) + 3J(\omega_N) + 6J(\omega_H + \omega_N)\} + cJ(\omega_N) \quad (3)$$

$$R_2 = \frac{d}{2}\{4J(0) + J(\omega_H - \omega_N) + 3J(\omega_N) + 6J(\omega_H) + 6J(\omega_H + \omega_N)\} + \frac{c}{2}\left[\frac{4}{3}J(0) + J(\omega_N)\right] \quad (4)$$

with $d = \gamma_H^2 \gamma_N^2 h^2/(2\pi)^2 4r_{NH}^6$ and $c = \Delta^2 \omega_N^2/3$. For a CSA value of $\Delta = -160$ ppm (Hiyama et al., 1988) and an internuclear ^{15}N−^{1}H bond distance of $r_{NH} = 1.02$ Å (Keiter, 1996), d and c become $\sim 1.3 \times 10^9$ (rad/s)^2 and 0.9×10^9 (rad/s)^2, respectively. On a 500 MHz spectrometer the relaxation rates R_1 and R_2 sample the spectral density function at the frequences $\omega = 0$ Hz, $\omega_N = 50.68$ MHz, $(\omega_H + \omega_N) = 449.46$ MHz, $\omega_H = 500.14$ MHz, and $(\omega_H - \omega_N) = 550.82$ MHz. In addition to R_1 or R_2 we use another parameter which is less sensitive toward internal motions in the time range of τ_m

$$2R_2 - R_1 = d\{4J(0) + 6J(\omega_H)\} + \frac{4}{3}cJ(0) \quad (5)$$

Lipari and Szabo (1982a,b) proposed a model for the autocorrelation function $G(t)$ and the spectral density function $J(\omega)$ on the basis of a minimal number of motional parameters:

$$G(t) = \frac{1}{5}S^2 \exp(-t/\tau_m) + \frac{1}{5}(1 - S^2)\exp(-t/\tau) \quad (6)$$

$$J(\omega) = \frac{2}{5}\left[\frac{S^2\tau_m}{1 + (\omega\tau_m)^2} + \frac{(1 - S^2)\tau}{1 + (\omega\tau)^2}\right] \quad (7)$$

with S^2, the order parameter, giving a measure for spatial restriction, τ_m the overall correlation time, and $1/\tau = 1/\tau_m + 1/\tau_e$, where τ_e is the effective correlation time and a function of the amplitude as well as of the frequency of the internal motion. This model is exact only if (1) the overall motion is isotropic, (2) the internal motion is much faster than τ_m, and (3) τ_e is defined as the area under the correlation function. In that case the overall correlation time can be extracted from the ratio R_2/R_1 on a residue by residue base by neglecting the second term of the spectral density function in eq 7 (Kay et al., 1989), and the error in τ_m can be estimated from the upper and lower limits of R_2/R_1. This reduced spectral density function together with the averaged value of τ_m can then be used to determine S^2 from eq 3 or 4 (Kay et al., 1989) or from eq 5 (Habazettl et al., 1995).

In Habazettl et al. (1995) a method was developed to obtain the most reliable values possible for the order parameter S^2 using R_1 and R_2 only, on the basis of the following considerations: Experimental results from ^{15}N relaxation experiments on proteins reported in the literature, in particular, the mapping of the spectral density function of the protein eglin c (Peng & Wagner, 1992), indicate that the spectral density function is largest at $J(0)$, $J(\omega_N)$ reaches values up to 50% of $J(0)$, and $J(\omega)$ is very small at high frequencies ($\omega \geq 449.46$ MHz). Unstructured terminal or loop regions are often exceptions and have broader spectral density functions (Peng & Wagner, 1992). In all cases, however, the prevailing terms in the relaxation rates of the more rigid parts of the protein are the spectral density functions at low frequencies. We therefore write expressions for R_1 and R_2 containing only $J(0)$ and $J(\omega_N)$ in order to examine how reliably such a simplification can reproduce order parameters S^2 from a more realistic synthetic data set for which the assumption of negligible spectral density functions at higher frequencies is not justified:

$$R_1 \approx (3d + c)J(\omega_N) \quad (8)$$

$$R_2 \approx \left(2d + \frac{2}{3}c\right)J(0) + \left(\frac{3}{2}d + \frac{1}{2}c\right)J(\omega_N) \quad (9)$$

$$2R_2 - R_1 \approx \left(4d + \frac{4}{3}c\right)J(0) \quad (10)$$

$$\frac{R_2}{R_1} \approx \frac{2}{3}\frac{J(0)}{J(\omega_N)} + \frac{1}{2} \quad (11)$$

It is apparent from eq 10 that the value of $2R_2 - R_1$ is mainly a function of $J(0)$. Thus, this expression is less sensitive to fast internal motions around the nitrogen frequency than R_1, R_2 or R_2/R_1. It is worth mentioning that, for small proteins with a correlation time of approximately 3 ns and at a spectrometer of 500 MHz proton frequency, $\omega_N\tau_c \approx 1$. Thus, R_1, R_2, or R_2/R_1 is sensitive to internal motions around the overall motion of the protein while $J(0)$ is much less sensitive to motions on this time scale.

Relaxation Rates R_1, $R_{1\rho}^{eff}$, and R_2. N-Ada10 shows good dispersion in the ^{15}N heteronuclear correlation spectrum (Figure 3). The relaxation rates for 76 amino acids out of 92 could be determined. The first three and the last three residues as well as residues His-46 and His-82 do not appear in the spectrum at all. Residues 21, 40, 68, 74, and 79 are prolines, and residues Glu-60, Lys-86, and Ile-87 are heavily overlapped. The rates R_1 and $R_{1\rho}^{eff}$, measured as described by Peng et al. (1992), and R_2, calculated from $R_{1\rho}^{eff}$, using eq 2, are displayed in the bar graphs of Figure 5. R_1 ranges from 1.1 to 2.1 s^{-1} and $R_{1\rho}^{eff}$ and R_2 from 2.2 to 15.2 s^{-1}. The rates show distinctively different relaxation behavior at the N- and C-terminal ends and at residues 25, 33−35, 45−48, 56, 72 and 73 from the rest of the protein. Neglecting these residues, the rates of the remaining 54 residues are quite uniform with an average value of $R_1 = 1.89 \pm 0.27$ s^{-1}, $R_{1\rho}^{eff} = 10.10 \pm 1.55$ s^{-1}, and $R_2 = 10.29 \pm 1.58$ s^{-1}. All 54 residues belong to the core of the protein. The residues of both termini, as well as residue Thr-34, and Ala-47 are distinguished by much smaller relaxation rates, R_1 and R_2. Residues Gly-25, Arg-45, Leu-48, and Cys-72 show a smaller rate for R_1 only. The R_2 rates of residues Gly-25 and Gln-73 are significantly (50%) larger than those of the rest of
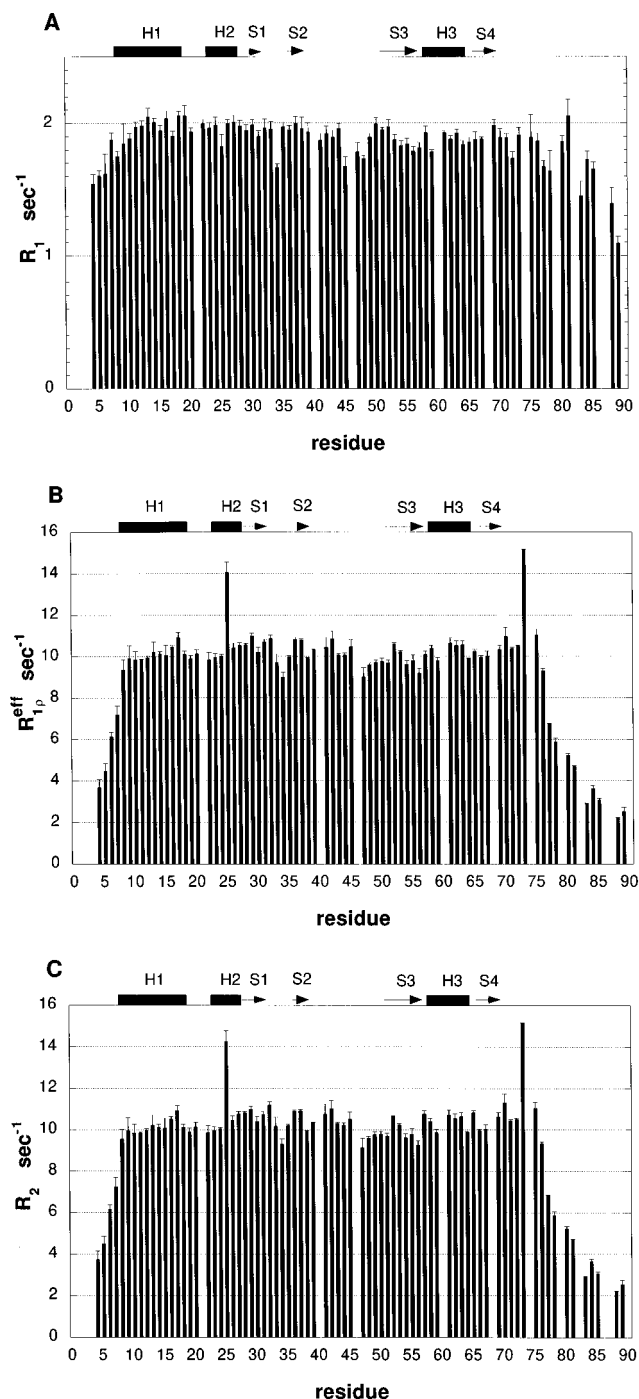
FIGURE 5: Bar graphs of the experimental ^{15}N R_1 (A), $R_{1\rho}^{eff}$ (B) , and R_2 (C) values versus the amino acid sequence for N-Ada10, recorded at 500 MHz and 25 °C. R_2 values were derived from $R_{1\rho}^{eff}$ rates, applying eq 2 in order to correct for resonance offset effects.

the protein. Such line widths suggest conformational and/ or solvent exchange processes. This includes exchange between different conformers occurring in these regions of the protein. The N-terminal end shows a monotonic increase from 3.7 s^{-1} at residue Ala-4 up to the average value of R_2 at residue Asp-9 and an almost monotonic increase from 1.5 s^{-1} for residue 4 to the average value of R_1 at residue Asp-10. At the C-terminal end, R_2 decreases from 11 s^{-1} at residue Asp-75 to 2.5 s^{-1} at residue His-89 and R_1 from 1.9 to 1.1 s^{-1}, respectively. Residues 1−7 and 74−92 appeared to form little well-defined secondary structure, as they have no medium- or long-range NOEs. Residues 1−4 and 88−92 did not even have short-range NOEs. Residues 33−35

are located in the turn of the two antiparallel β-strands, S1 and S2. Residues 45−50 are in the loop which connects metal-ligated cysteines 38 and 42 with antiparallel β-strand S3. Ala-56 is located at the transition point where the anti parallel β-strand converts into helix H3. Residue 25 is located in the beginning of a short helix, H2, which connects helix H1 with the first β-strand, S1. The other residues of H2 and also of the following S1 do not show any distinctive relaxation behavior. Gln-73 follows Cys-72, which coordinates the zinc ion. The less well-defined C-terminal end of the protein begins at residue 73, as shown by the lack of medium- and long-range NOEs.

Order Parameter S^2. The R_2/R_1 ratios for every residue are shown in Figure 6A. If there were no or only fast internal motions in the range of picoseconds, R_2/R_1 would be uniform for all residues. Internal motions in the time range of τ_m will reduce this value, while any conformational and/or solvent exchange process will enlarge it. Such a chemical exchange process can be due to conformational exchange in the time range from milliseconds to nanoseconds or/and due to fast exchange of the amide proton with solvent. In order to determine τ_m from R_2/R_1 (Kay et al., 1989), it is important to choose quite rigid N−H vectors which do not undergo any conformational and/or solvent exchange processes. The ratios of residues 61−64 were chosen for this purpose. These four residues are adjacent in the primary sequence and are located in the middle of α-helix H3. All four residues are involved in hydrogen bonds and show very long backbone amide exchange times with solvent even though the helix is located at the surface of the protein. Their ratio values are quite high and the corresponding errors relatively small. The mean ratio of R_2/R_1 averaged over residues 61−64 is 5.50 ± 0.13. The range from 5.37 to 5.63 is indicated in the figure by horizontal solid lines. On the basis of these residues the time constant of the overall tumbling resulted in $\tau_m = 8.09 \pm 0.15$ ns. The values at the N- and C-terminal ends of the protein are much smaller. Residues Gly-25, Arg-45, Cys-72, and Gln-73 have significantly higher values for R_2/R_1 ratios outside their error limits. Such behavior suggests an additional exchange process, due to conformational exchange and/or solvent exchange which causes this line broadening. It is interesting to point out that for Cys-72 this was not obvious from the R_2 value alone. For other residues this value is high as well; however, the error limits are too high to be certain (Asn-57, Gly-65, and Lys-70). Most residues of α-helix H1, residues 22−24, 35, and 49−51, have significantly smaller R_2/R_1 values than the average of 5.50 ± 0.13, suggesting internal motions in the time range of τ_m. For the rest of the protein the deviations of R_2/R_1 from 5.50 ± 0.13 are within the error limits. Residues 22−24 are located at the beginning of H2, residue 35 is in the turn between the two antiparallel β-sheets, S1 and S2, and residues 49−51 are at the end of the loop between S2 and S3.

The order parameters calculated from eq 5 together with the first term of eq 7 with $\tau_m = 8.09 \pm 0.15$ ns are displayed in Figure 6B versus the amino acid sequence. The error limits are calculated from the error estimates for R_1, R_2, and τ_m. The apparent order parameters for Gly-25 and Gln-73 are larger than unity due to conformational and/or solvent exchange. Figure 6B shows noticeably smaller order parameters for the residues at the N- and C-terminal end of the protein, an internal stretch from residue 47 to residue 51, and two "dips" at residues 33−35 and 54−56. The first
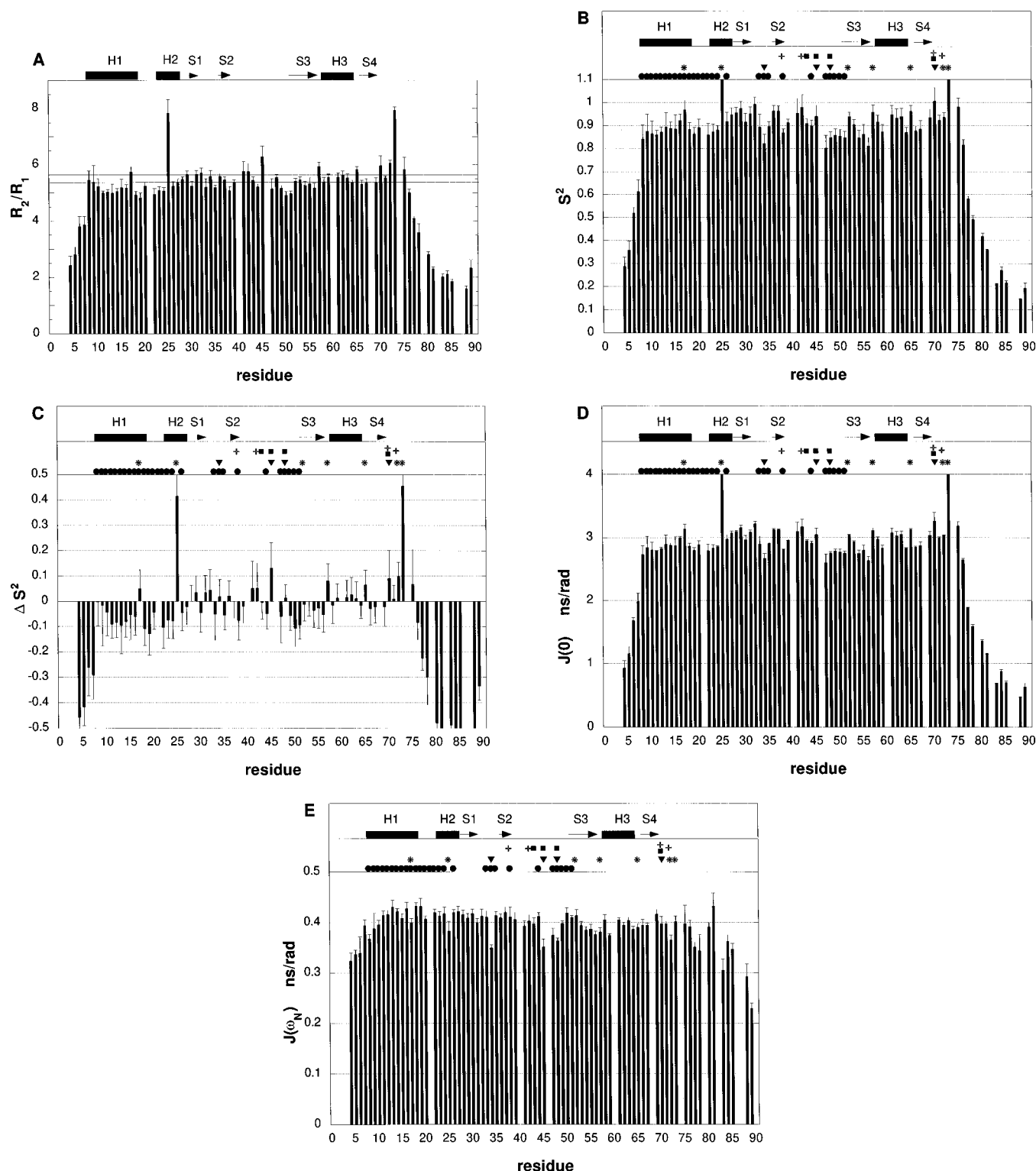
FIGURE 6: Experimental values of R_2/R_1 (A), the order free parameter S^2 derived from $2R_2 - R_1$ values (B), the difference between the order parameters derived from $2R_2 - R_1$ and R_1 (C), $J(0)$ derived from eq 10 (D), and $J(\omega_N)$ derived from eq 8 versus amino acid sequence of the backbone amide nitrogens of N-Ada10 (E). The standard deviation of every value is indicated above each bar. In (A) the horizontal lines show the range of R_2/R_1 averaged over residues Ala-61, Leu-62, Ala-63, and Ala-64 with $\langle R_2/R_1 \rangle = 5.50 \pm 0.13$. On the basis of this value the overall correlation time τ_m was calculated with $\tau_m = 8.09 \pm 0.15$ ns. Using this estimate of τ_m the values of S^2 in (B) were determined. The error limits for S^2 are the standard deviations based on the errors of R_1, R_2, and τ_m. Above the S^2 bars residues which suggest motional components in the time range of τ_m are indicated by (●), slow conformational exchange processes by (*), conformational and/or solvent exchange by (▼), the four zinc binding cysteines by (+), and residues whose side chains show a change in amide ^{15}N or NH chemical shifts after the addition of a 12-mer duplex oligodeoxinucleotide by (■).

dip from residues 33−35 is located in the turn between antiparallel β-strands S1 and S2, residues 47−51 are at the end of the loop between S2 and S3, with Asn-51 already part of S3, and residues 54−56 are at the end of β-strand S3 and where S3 turns into the helix H3. The remaining

N−NH vectors have much more uniform order parameters, ranging from 0.87 to 0.97 and with an average of 0.90.

The differences between the order parameters determined from the $2R_2 - R_1$ values [$S^2(2R_2 - R_1)$] and from the R_1 values [$S^2(R_1)$] are displayed in Figure 6C. $S^2(R_1)$ was

calculated using eq 3 and the first term of eq 7 and $S^2(2R_2 - R_1)$ using eq 5 and the first term of eq 7 with $\tau_m = 8.09 \pm 0.15$ ns . In the case of internal motions in the time range of τ_m the order parameter $S^2(R_1)$ is overestimated and larger than $S^2(2R_2 - R_1)$ (Habazettl & Wagner, 1995). If there is a conformational or solvent exchange process resulting in line broadening, $S^2(2R_2 - R_1)$ is too large. Comparison of ΔS^2 with R_2/R_1 shows that the motional pictures emerging from the two parameters are identical. It also indicates that $2R_2 - R_1$ is less susceptible to motions in the time range of τ_m than R_1 and is therefore better suited for calculating S^2. The spectral density functions at the frequencies 0 and ω_N were calculated by applying the approximations of eqs 8 and 10 and are shown in panels D and E of Figure 6, respectively. Errors due to these approximations are not included in the error estimates given in these plots. As $J(0) \gg J(\omega_H)$, neglecting $J(\omega_H)$ in eq 10 should result in only very small errors, whereas increased line broadening due to conformational and/or solvent exchange can result in quite large errors and cannot be neglected. The neglect of contributions of $J(\omega_H \pm \omega_N)$ to R_1 is more severe. Nevertheless, comparing $J(0)$ and $J(\omega_N)$ with those of eglin c (Peng & Wagner, 1992b) shows that $J(0)$ of N-Ada10 is approximately twice the value of eglin c, whereas $J(\omega_N)$ is in the same range for both proteins. This reflects the fact of τ_c of N-Ada10 being about twice the correlation time of eglin c and $J(0)$ being directly proportional to τ_c in a first approximation.

Conformational Exchange Rate of Glu-73. One of the four cysteines involved in the binding of zinc shows different motional behavior: Cys-72 and its neighboring residue, Gln-73, are more mobile and show a slow conformational process. The contribution of a conformational exchange process to $R_{1\rho}$ can be determined if the frequency of this exchange process is near the Larmor frequency of the RF spin-lock field ω_1. For a system of nuclei exchanging randomly between two conformational states with arbitrary populations $R_{1\rho}$ is given by (Deverell et al., 1970)

$$R_{1\rho} = K \frac{\tau_{ex}}{1 + (\omega_1 \tau_{ex})^2} + R_{1\rho}^{\infty} \qquad (12)$$

with $K = p_A p_B \Delta\Omega^2$, p_A and p_B are the population of states A and B, respectively, $\Delta\Omega^2$ is the chemical shift difference between states A and B, ω_1 is the Larmor frequency of the applied spin-lock field, $R_{1\rho}^{\infty}$ the relaxation rate for an infinitely large spin-lock power, and τ_{ex} is the time constant of the conformational exchange process. To study Gln-73, the carrier was placed on-resonance so that off-resonance effects could be neglected.

The transverse relaxation rates of Glu-73 are shown in Figure 7 as a function of the applied RF spin-lock field ω_1. The solid squares and circles represent the experiments performed with and without decoupling protons with Waltz-16, respectively, during the transverse relaxation of ^{15}N. Applying proton decoupling improved the experimental performance. The frequency of the conformational exchange process lies in the experimentally sampled frequency range. The solid line represents the least squares fit of the data points with eq 12, setting $R_{1\rho}^{\infty}$ to the average value of $R_{1\rho}$, 10.10 s^{-1}. The frequency ω_1 at the turning point of the curve represents $1/\tau_{ex}$. The fit resulted in a value of $\tau_{ex} = 60.56 \pm 5 \mu$s.

Backbone Amide Proton Exchange with Solvent. The amide proton exchange times for N-Ada10 are shown in
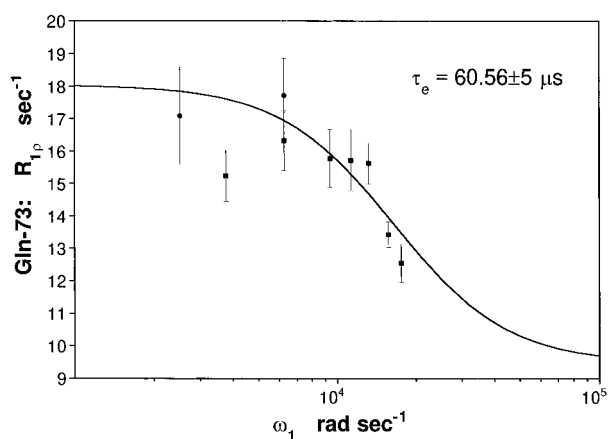

FIGURE 7: Plot of the experimental transverse relaxation rate $R_{1\rho}$ of Glu-73 versus the applied spin-lock power H_1 during transverse relaxation of ^{15}N. The data points with solid squares were measured with pulse sequence 4A and the solid circles with 4B, respectively. The solid curve represents the least squares fit with the function of eq 12. The two data points acquired with pulse sequence 4A at low spin-lock power were not used in the fit. For an error estimation of τ_{ex} the fit was repeated with the upper error limits of the data points and the lower error limits.
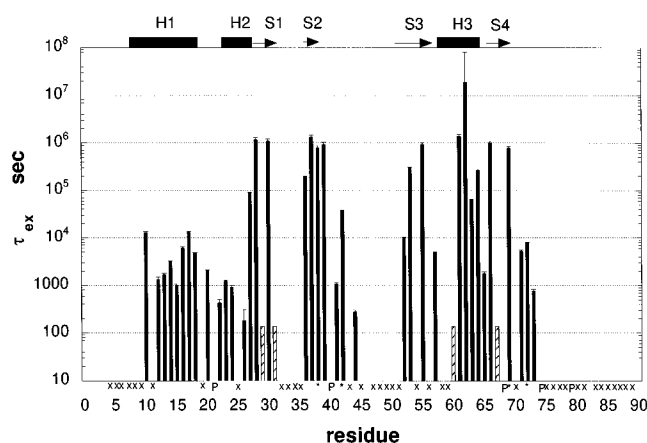

FIGURE 8: Bar graph of the backbone amide proton exchange times in N-Ada10 versus the amino acid sequence. The time constants were determined using ^{1}H$-^{15}$N heteronuclear correlation NMR spectroscopy. A total of 120 time points were collected within the first 2 days at a temperature of 25 °C. The estimated error of every value is indicated above each bar. The hatched bars represent those residues whose amide proton is seen in the first HSQC spectra but whose exchange time could not be determined due to heavy overlap. Residues whose amide proton cannot be seen in the first HSQC spectrum acquired after initiation of exchange out are indicated with (x), the zinc binding cysteines with (*), and the prolines with (P).

Figure 8. The first three and the last three residues as well as residues 46 and 82 do not show up in the HSQC spectrum in water at all, and residues 21, 40, 68, 74, and 79 are prolines. For N-Ada10, at 25 °C and pH 6.4, 41 backbone amide protons exchanged sufficiently slowly with solvent to be seen in the first HSQC spectrum acquired after initiation of exchange out. The solvent exchange time could be determined quantitatively for 36 out of 41 residues. Residues Phe-29, Val-31, Glu-60, and Arg-67 appear in the spectra, but their solvent exchange time could not be determined due to heavy resonance overlap. A lower limit for the solvent exchange time of 160 s can be estimated for these residues. The errors for the solvent exchange times of residues 10 and 17 may be underestimated due to slight overlap. The resonance of the amide proton Glu-26 was seen only in the first regular HSQC spectrum and has decayed to the level of noise in the second. Its time constant can be estimated

within the range of 160−300 s. In summary, the amide protons of residues 10, 12−18, 20, 22−24, 26−31, 36−39, 41, 42, 44, 52, 53, 55, 57, 60−67, 69, and 71−73 are slowly exchanging with solvent. An upper limit of 220 s can be given for those residues, whose amide proton has exchanged within the first 12 min with solvent and cannot be seen in the first HSQC spectrum: residues 4−9, 11, 19, 32−35, 43, 45, 47−51, 54, 56, 58, 59, 70, and 76−92. The resonances of Gly-25 and Asp-75 are very weak in the HSQC spectrum in water and cannot be seen in the first spectrum after the initiation of exchange out. An upper limit of 300 s can be given for these resonances. Most of the slowly exchanging backbone amide protons are involved in secondary structure elements or are grouped around the zinc binding cysteines, Cys-38, Cys-42, Cys-69, and Cys-72. The slowest solvent exchange processes take place at residues 28, 30, 37−39, 55, 61, 62, 66, and 69. They are part of the secondary structure elements with the exception of residue 39. Residues Cys-38 and Cys-69 are two out of the four zinc binding cysteines, and residues 37 and 39 are direct neighbours of Cys-38.

DISCUSSION

Determination of τ_m. The ratio of R_2/R_1 is independent of the amplitude of the internal motions at much faster and much slower motions than τ_m; it is reduced by internal motions in the time range of τ_m and increased by conformational and/or solvent exchange processes. The ratio of R_2/R_1 is used for many purposes. First, it is used either to calculate the final overall correlation time τ_m or to use the so-derived value of τ_m as a first guess in the model-free approach fitting procedures. The value of τ_m calculated in this way is correct only if the internal motions are either much faster or much slower than τ_m and no conformational and/or solvent exchange processes take place. In the case of internal motions in the time range of τ_m this may lead to a systematic error toward shorter τ_m. On the other hand, τ_m would be overestimated in cases of decay processes that contribute significantly to R_2 (conformational and/or solvent exchange). One way to overcome these uncertainties is to use R_2/R_1 values of residues that are involved in secondary structure elements (Kay et al., 1989) or to exclude all those values from calculating τ_m that are outside ±1 standard deviation from mean (Clore et al., 1990b). Comparing the plots of ratios of R_2/R_1 of different proteins shows that these values tend to be higher in regular secondary structure elements than in loops showing that residues involved in secondary structure are more rigid. However, Rischel et al. (1994) observed that part of an α-helix of the acyl-coenzyme A binding protein became more rigid upon ligand binding. This suggests that secondary structure elements nevertheless can be quite flexible and τ_m determined from their R_2/R_1 value may be underestimated. Another use of R_2/R_1 ratios was suggested by Clore et al. (1990b). This criterion is used to decide if slow internal motions in the time range of τ_m or conformational and/or solvent exchange processes are taking place: If the ratio of R_2/R_1 is less than one standard deviation from the mean, internal motions are assumed in the time range of $\approx 0.001\tau_m$ and $\approx 0.1\tau_m$. The relaxation parameters are then fitted with the extended model-free approach, which employs a double exponential function for representing the autocorrelation function of the internal motions (Clore et al., 1990). For R_2/R_1 values of one standard deviation more than the mean, conformational and/or solvent exchange processes

are assumed to take place, and the experimental data are fitted with an additional term in the extended model-free approach (Clore et al., 1990). If one has a systematic error in τ_m toward a smaller value, this could result in interpreting a very rigid N−H vector as undergoing a conformational and/or solvent exchange processes or, on the other hand, in underestimating the actual mobility of the whole protein. If an N−H vector undergoes conformational and/or solvent exchange and has motions in the time range of τ_m, one effect can cancel the other and may result in an R_2/R_1 value typical for residues with very fast internal motions. For example, different groups have found conformational and/or solvent exchange processes in supposedly rigid secondary structure elements (Powers et al., 1992; Redfield et al., 1992). Considering all the problems in deciding which R_2/R_1 values are the best for calculating τ_m, we use the NH exchange data as an additional criterion: (1) involvement in hydrogen-bonding network of a regular secondary structure, (2) at least three neighboring residues in the primary sequence with relatively high R_2/R_1 values and small errors, and (3) very long NH exchange times. Only residues 61−64 fulfill all these criteria. They are located in the helix which emerges from an antiparallel β-strand and goes over into another antiparallel β-strand that is fixed by a covalent bond of Cys-69 to the zinc ion. The average value of R_2/R_1 of these 4 residues is 5.5 ± 0.13, and its range is indicated in Figure 6A by the two horizontal lines. The value calculated from these residues resulted in $\tau_m = 8.09 ± 0.15$ ns. The different time points for determining R_1 were acquired in random order. For control the first time point acquired was repeated at the end to the time series. The intensity of this first time point had decreased by 2%. Therefore, in order to determine a more accurate τ_m from R_2/R_1, it is advisable to perform the R_1 and R_2 experiments all interleaved. One also has to ascertain if the overall molecular tumbling is isotropic. The principal components of the tensor of inertia of N-Ada10 including all residues vary within a wide range for every structure shown in Figure 1. However, the N- and C-terminal ends of the protein are not structured and can be excluded. This leads to a ratio of 1:0.88:0.94 and shows that the assumption of isotropic tumbling is a good approximation.

Interpretation of the Relaxation Parameters. Due to the reduced sensitivity of the NOE experiment and/or protein instability different groups determined S^2 from R_1 or R_2 alone and used the NOE enhancement for qualitative purposes only (Kay et al., 1989; Rischel et al., 1994). As N-Ada10 is not very stable in solution and an NOE experiment typically lasts 1 week, we did not determine the NOE enhancement at all and determined the order parameter from $2R_2 - R_1$ (Habazettl & Wagner, 1995). Conformational and/or solvent exchange contributions, however, would increase the so-determined value of S^2. Therefore, the order parameters have to be used with caution, and only a careful analysis including NH exchange data and the R_2/R_1 values can give insight into the different possible internal motions. Figure 6B gives a summary of the motional picture of the protein. On the top of the figure are indicated those residues where we think significant motions in the time scale of τ_m take place and/or where significant line broadening due to NH exchange with the solvent and/or chemical exchange between different conformers occurs. In the case of line broadening the shown order parameter below is too large; in the case of motions in the time scale of τ_m the values of the order parameters might be overestimated. As conformational and/or solvent

exchange processes may hide a motional component in the time range of τ_m, we assume that such motions are present if both residues adjacent in the primary sequence also showed reduced R_2/R_1 values. In Figure 1B, those residues are shown in magenta for which we have indication of motion around the time scale of τ_m. It appears that they form an almost contiguous wedge on one side of the protein. This observation was rather unexpected and will be the subject of further studies. It is also of interest whether similar observations of motional clustering will be seen in other proteins.

Residues 10–31 excluding residues 11, 19, and 25 have quite long NH exchange times, and therefore an increase of R_2 due to NH exchange can be excluded. Residues 10–26 excluding Leu-17 and Gly-25 tend to have R_2 values comparable to the core of the protein but shorter R_1 values. This results in a reduced R_2/R_1 value and suggests some slow motional components with correlation times in the time range of $0.01\tau_m$ to $0.1\ \tau_m$. Residues 8 and 9 have relatively large errors, and their R_2 values might also have contributions from solvent exchange. Residue Leu-17 has a relatively small R_1 rate but larger R_2 rate than the other residues of helix H1. The R_2/R_1 value for this residue does not exceed the error limits of $\langle R_2/R_1 \rangle = 5.50 \pm 0.13$, but it is significantly larger than for the other residues of helix H1. Altogether, it seems that the residues of helix H1 at the N terminal end, the loop connecting H1 and H2, and the beginning of helix H2 have motional components in the time range of τ_m while residues 17 and 25 have even conformational and/or solvent exchange processes. The order parameters S^2 for these residues might be overestimated, depending on the time range of the internal motions. Helix H1 does not seem to have hydrogen bonds or salt bridges to the rest of the protein. It is stabilized only by some of its side chains that are involved in a hydrophobic core consisting of the side chains of residues Phe-54, Phe-27, Phe-29, Trp-13, Leu-17, and Val-16.

Of the four ligand binding cysteines one residue, Cys-72, shows a slow conformational exchange process, and Cys-42 might undergo such a process as well, but the error limits are too large for this residue to be certain. Cys-38 seems to have motional components in the time range of τ_m, and residue 69 is quite rigid. Even though these four residues are connected through covalent bonds of their side chains with the zinc ion, they show motions on different time scales. The conformational and/or solvent exchange process of Cys-72 might also be due to the truncation of the protein. Similar observations, however, were made for the residues involved in binding zinc in the zinc finger DNA binding domain from Xfin (Palmer et al., 1991). In contrast, the two Ca^{2+} binding loops of calcium-loaded calbindin do not show conformational and/or solvent exchange processes and no increased amplitude of motion (Kördel et al., 1992). However, Grasberger et al. (1993) observed line broadening for residues connected through hydrogen bonds and buried hydrophobic side chains and concluded concerted movements for such a cluster.

Relations between Relaxation Rates, NH Exchange, and Structural Definition. Motions relevant for nitrogen relaxation and amide proton exchange are expected to be on different time scales. Thus, indeed, little correlation has been found in the past between hydrogen exchange rates and nitrogen relaxation rates or molecular dynamics simulations that would cover events at the relaxation rate time scale [see, for example, Wagner (1983)]. However, earlier comparisons were made on the basis of much less detailed analysis of
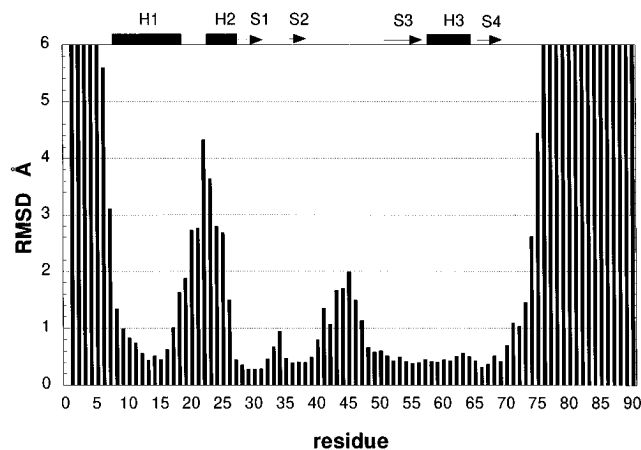

FIGURE 9: Average RMSD per residue of the heavy backbone atoms determined from pairwise fits of the 14 individual structures shown in Figure 1. The fits included the well-defined parts of the protein: residues 8–17, 27–41, and 49–73.

relaxation data. Thus, a comparison is worthwhile for a situation where spectral density data are available, such as for Nada10. Here, all residues for which motions on the time scale of τ_m or indications of slower structural fluctuations were found have NH exchange times shorter than 2×10^4 s. On the other hand, not all residues that are rigid as indicated from relaxation rates have slow NH exchange. The exception is Cys-38, with indications for motions on the time scale of τ_m and a very long NH exchange time. It is interesting to point out that Cys-38 is one of the four cysteines to which Zn^{2+} is tetrahedrally coordinated. Residue 38 is located opposite to Cys-72, which undergoes a slow conformational exchange process. Arg-45 and Lys-70 have line broadening due to conformational and/or solvent exchange and also have short NH exchange times. The R_2/R_1 ratios of Ser-41 and Cys-42 also indicate conformational and/or solvent exchange processes, but the error limits for these residues are quite large. Nevertheless, the NH exchange time of Ser-41 is short. The Cys-42 NH exchange constant of 5×10^4 s is quite long. This residue is also one of the four zinc binding cysteines.

N-Ada10 is not structured at the N- and C-terminal ends. The antiparallel β-strands S1, S2, S3, and S4 as well as the α-helix H3 are well defined and correlate well with the areas of the protein of fast internal motion. Three residues of the loop connecting S1 with S2 have increased RMSD values (Figure 9), smaller order parameters, and motions on the time scale of τ_m. Residues 40–47 show high RMSD values and are located in the loop between S2 and S3. Comparing the NH exchange rates and the order parameters, one would expect the range from residue 40 to residue 44 to be better defined. Also, the NH exchange rates and the relaxation experiments of residues 16–26 do not indicate the poor definition of this range due to mobility. Therefore, the poor definition of these regions is not due to high mobility but rather is a result of geometrical factors. Kördel et al., (1992) made similar observations with the Ca^{2+} loops in Ca^{2+}-loaded calbindin D_{9k}, whereas the structure of the zinc finger DNA binding domain from Xfin (Palmer et al., 1991) was well defined.

What Can We Conclude for the Function of Ada? Ada repairs methyl phosphotriesters in DNA by direct, irreversible methyl transfer to Cys-69. Upon methyl transfer, Ada acquires the ability to bind specific DNA sequences. It was shown that the four zinc binding cysteines retain coordinate

bonds with the metal after the acceptance of the methyl group at Cys-69 (Ohkubo et al., 1994; Myers et al., 1994). This result suggested that the DNA binding ability is acquired by a relatively small conformational change or by the direct contact of the added methyl group with the cognate DNA sequence. The role of Zn^{2+} may be viewed as an anchor that controls the correct positioning of the *S*-methyl group upon DNA binding. The question remains if certain mobility of the residues which are close to the zinc is important for (1) the methyl transfer to Cys-69 and/or (2) the specific DNA binding. Relaxation studies have been done on three DNA binding molecules which also bind zinc: GAL4 (Lefèvre et al., 1996), Xfin (Palmer et al., 1991), and N-Ada10. In all three proteins the four residues which bind the zinc show motions on different time scales ranging from microsecond to picosecond. As the Ca^{2+} binding loops of Ca^{2+}-loaded calbindin D_{9k} (Kördel et al., 1992) are quite rigid, it seems possible that the aforementioned motional characteristics of GAL4, Xfin, and N-Ada10 are necessary for the DNA binding.

The identification of Cys-69 as a zinc ligand implicated that the zinc ion not only served to stabilize the protein structure but also participated in the direct metalloactivation of the methyl acceptor residue (Myers et al., 1993). Other proteins that possess zinc-bound thiolates may be designed to suppress their intrinsic reactivity by hydrogen bonds of mainly backbone amide protons to the coordinated sulfur atoms, thereby decreasing the negative charge density on the ligand and its nucleophilicity (Blake & Summers, 1993). The improved amide proton exchange data presented in this paper show that amide protons in the residues near the sulfur atoms are slowly exchanging. Considering the relatively poor structural definition of N-Ada10 around Cys-38, Cys-42, and Cys-72, possible hydrogen bonds cannot be uniquely identified from the ensemble of structures: there may exist different hydrogen bonds between close amide protons and the four zinc binding sulfurs in different structures. Therefore, decrease of the nucleophilicity by hydrogen bonds to the coordinated sulfur atoms cannot be excluded for Ada. To gain insight into the mechanisms of the structure-function relations of Ada, works on refining the structure of N-Ada10 and also structural studies of the protein−DNA complex are in progress.

SUPPORTING INFORMATION AVAILABLE

A table with the chemical shifts for the assigned proton, nitrogen, and carbon resonances of N-Ada10 at 25 °C (3 pages). Ordering information is given on any current masthead page.

REFERENCES

Abragam, A. (1961) *The Principles of Nuclear Magnetism*, Clarendon Press, Oxford, England.

Barbato, G., Ikura, M., Kay, L. E., Pastor, R. W., & Bax, A. (1992) *Biochemistry 31*, 5269−5278.

Bax, A., & Ikura, M. (1991) *J. Biomol. NMR 1*, 99−104.

Bodenhausen G., & Ruben, D. J. (1980) *Chem. Phys. Lett. 69*, 185−199.

Brown, S. C., Weber, P. L., & Mueller, L. (1988) *J. Magn. Reson. 77*, 166−169.

Carr, H. Y., & Purcell, E. M. (1954) *Phys. Rev. 94*, 630.

Clore, G. M., Szabo, A., Bax, A., Kay, L. E., Driscoll, P. C., & Gronenborn, A. M. (1990a) *J. Am. Chem. Soc 112*, 4989- 4991.

Clore, G. M., Driscoll, P. C., Wingfield, P. T., & Gronenborn, A. M. (1990b) *Biochemistry 29*, 7387−7401.

Davis, D. G., & Bax, A. (1985) *J. Am. Chem. Soc. 107*, 2820−2821.

Davis, D. G., Perlman, M. E., & London, R. E. (1994) *J. Magn. Reson. B 104*, 266−275.

Dellwo, M. J., & Wand, A. J. (1989) *J. Am. Chem. Soc. 111*, 4571−4578.

Demple, B. (1990) in *Protein Methylation* (Paik, W. K., & Kim, S., Eds.) pp 285−304, CRC Press, Boca Raton, FL.

Deverell, C., Morgan, R. E., & Strange, J. H. (1970) *Mol. Phys. 18*, 553−559.

Englander, S. W., & Kallenbach, N. R. (1984) *Q. Rev. Biophys. 16*, 521−655.

Fesik, S. W., & Zuiderweg, E. R. P. (1988) *J. Magn. Reson. 78*, 588−593.

Fushman, D., Weisemann, R., Thüring, H., & Rüterjans, H. (1994) *J. Biomol. NMR 4*, 61−78.

Grasberger, B. L., Gronenborn, A. M., & Clore, G. M. (1993) *J. Mol. Biol. 230*, 364−372.

Grzesiek, S., & Bax, A. (1992) *J. Magn. Reson. 96*, 432−440.

Habazettl, J., & Wagner, G. (1995) *J. Magn. Reson. B 109,* 100−104.

Kay, L. E., Torchia, D. A., & Bax, A. (1989) *Biochemistry 28*, 8972−8979.

Kay, L. E., Ikura, M., Tschudin, R., & Bax, A. (1990) *J. Magn. Reson. 84*, 496−514.

Kay, L. E., Nicholson, L. K., Delaglio, F., Bax, A., & Torchia, D. A. (1992) *J. Magn. Reson. 97*, 359−375.

Keiter, E. A. (1986) Ph.D. Thesis, University of Illinois.

Kinosita, K., Kawato, S., Jr., & Ikegami, A. (1977) *Biophys. J. 20*, 289−305.

Kördel, J., Skelton, N. J., Akke, M., Palmer, A. G., III, & Chazin, W. J. (1992) *Biochemistry 31*, 4856−4866.

Lefèvre, J.-F., Dayie, K. T., Peng, J. W., & Wagner, G. (1996) *Biochemistry 35*, 2674−2686.

Lindahl, T., Sedgewick, B., Sekiguchi, M., & Nakabeppu, Y. (1988) *Annu. Rev. Biochem. 57*, 133−157.

Lipari, G., & Szabo, A. (1982a) *J. Am. Chem. Soc. 104*, 4546−4559.

Lipari, G., & Szabo, A. (1982b) *J. Am. Chem. Soc. 104*, 4559−4570.

Marion, D., & Wüthrich., K. (1983) *Biochem. Biophys. Res. Commun. 113*, 967−974.

Marion, D., Ikura, M., & Bax, A. (1989) *Biochemistry 28*, 6150−6156.

Marquardt, D. W. (1963) *J. Soc. Ind. Appl. Math. 11*, 431−441.

Meiboom, S., & Gill, D. (1958) *Rev. Sci. Instrum. 29*, 688.

Messerle, B. A., Wider, G., Otting, G., Weber, C., & Wüthrich, K. (1989) *J. Magn. Reson. 85*, 608−613.

Mierlo, C. P. M., Darby, N. J., Keeler, J., Neuhaus, D., & Creighton, T. E. (1993) *J. Mol. Biol. 229*, 1125−1146.

Montelione, G. T., Winkler, M. E., Rauenbuehler, P., & Wagner, G. (1989) *J. Magn. Reson. 82*, 198−204.

Müller, N., Ernst, R. R., & Wüthrich, K. (1986) *J. Am. Chem. Soc. 108*, 6482−6492 .

Myers, L. C., Terranova, M. P., Nash, H. M., Markus, M. A., & Verdine, G. L. (1992) *Biochemistry 31*, 4541−4547.

Myers, L. C., Terranova, M. P., Ferentz, A. E., Wagner, G., & Verdine, G. L. (1993a) *Science 261*, 1164−1167.

Myers, L. C., Verdine, G. L., & Wagner, G. (1993b) *Biochemistry 32*, 14089−14094.

Myers, L. C., Cushing, T. D., Wagner, G., & Verdine, G. L. (1994) *Chem. Biology 1*, 91−97.

Myers, L. C., Jackow, F., & Verdine, G. L. (1995) *J. Biol. Chem. 270*, 6664−6670.

Neri, D., Szyperski, T., Otting, G., & Wüthrich, K. (1989) *Biochemistry 28*, 7510−7516.

Nirmala, N. R., & Wagner, G. (1988) *J. Am. Chem. Soc. 110*, 7557−7558.

Nowak, U. K., Li, X., Teuten, A. J., Smith, A. G., & Dobson, C. M. (1993) *Biochemistry 32*, 298−309.

Ohkubo, T., Sakashita, H., Sakuma, T., Kainosho, M., Sekiguchi, M., & Morikawa, K. (1994) *J. Am. Chem. Soc. 116*, 6035−6036.

Palmer, A. G., III, Rance, M., & Wright, P. E. (1991) *J. Am. Chem. Soc. 113*, 4371−4380.

Palmer, A. G., III, Skelton, N. J., Chazin, W. J., Wright, P. E., & Rance, M. (1992) *Mol. Phys. 75*, 699−711.

Peng, J. W., & Wagner, G. (1992a) *J. Magn. Reson. 98*, 308−332.

Peng, J. W., & Wagner, G. (1992b) *Biochemistry 31*, 8571−8568.

Peng, J. W., & Wagner, G. (1994a) *Methods Enzymol. 239*, 563−596.

Peng, J. W., & Wagner, G. (1994b) in *NMR Probes of Molecular Dynamics* (Tycko, R., Ed.) pp 373−454, Kluwer Academic Publishers, Dordrecht.

Peng, J. W., Thanabal, V., & Wagner, G. (1991) *J. Magn. Reson. 95*, 421−427.

Piantini, U., Sørensen, O. W., & Ernst, R. R. (1982) *J. Am. Chem. Soc. 104*, 6800−6801.

Powers, R., Clore, G. M., Stahl, S. J., Wingfield, P. T., & Gronenborn, A. (1992) *Biochemistry 31*, 9150−9157.

Press, W. H., Flannery, B. P., Teukolsky, S. A., & Vetterling, W. T. (1988) *Numerical Recipes in C−The Art of Scientific Computing*, Cambridge University Press, New York.

Redfield, C., Boyd, J., Smith, L. J., Smith, R. A. G., & Dobson, C. M. (1992) *Biochemistry 31*, 10431−10437.

Rischel, C., Madsen, J. C., Andersen, K. V., & Poulsen, F. M. (1994) *Biochemistry 33*, 13997−14002.

Sakashita, H., Sakuma, T., Ohkub, Kainosho, M., Sakumi, K., Sekiguchi, M., & Morikawa, K. (1993) *FEBS Lett. 323*, 252−256.

Schneider, D. M., Dellwo, M. J., & Wand, A. J. (1992) *Biochemistry 31*, 3645−3652.

Senn, H., Werner, B., Messerle, B. A., Weber, C., Traber, R., & Wüthrich, K. (1989) *FEBS Lett. 249*, 113−118.

Shaka, A. J., Keeler, J., Frenkiel, T., & Freeman, R. (1983) *J. Magn. Reson. 52*, 335−338.

Shaka, A. J., Barker, P. B., & Freeman, R. (1985) *J. Magn. Reson. 64*, 547−552.

Skelton, N. J., Palmer, A. G., III, Akke, M., Kördel, J., Rance, M., & Chazin, W. J. (1993) *J. Magn. Reson. B 102*, 253−264.

Stone, M. J., Fairbrother, W. J., Palmer, A. G., III, Reizer, J., Saier, M. H., Jr., & Wright, P. E. (1992) *Biochemistry 31*, 4394−4406.

Stone, M. J., Chandrasekhar, K., Holmgren, A., Wright, P. E., & Dyson, H. J. (1993) *Biochemistry 32*, 426−435.

Szyperski, T., Neri, D., Leiting, B., Otting, G., & Wüthrich, K. (1992) *J. Biomol. NMR 1*, 99−104.

Szyperski, T., Luginbühl, P., Otting, G., Guntert, P., & Wüthrich, K. (1993) *J. Biomol. NMR 3*, 191−164.

Wagner, G. (1983) *Q. Rev. Biophys. 16*, 1−57.

Wagner, G. (1993) *Curr. Opin. Struct. Biol. 3*, 748−754.

Wagner, G., & Nirmala, N. R. (1989) *Chem. Scr. 29A*, 27−30.

Woessner, D. E. (1962) *J. Chem. Phys. 36*, 1−4.

Zink, T., Ross, A., Lüers, K., Cieslar, C., Rudolph, R., & Holak, T. A. (1994) *Biochemistry 33*, 8453−8463.

Zuiderweg, E. R. P. (1990) *J. Magn. Reson. 78*, 533−542.